OPEN

PRS GLOBAL OPEN

EXPERIMENTAL

Therapeutic Reversal of Radiotherapy Injury to Pro-fibrotic Dysfunctional Fibroblasts In Vitro Using Adipose-derived Stem Cells

Lipi Shukla, MBBS, Dip Anat Surg, PhD*†‡§
Rodney Luwor, BSc, PhD¶
Matthew E. Ritchie, BSc(Hons), PhD‖
Shiva Akbarzadeh, BSc, PhD§
Hong-Jian Zhu, BSc, PhD¶
Wayne Morrison, MD, FRACS*†‡
Tara Karnezis, BSc(Hons), PhD*†‡
Ramin Shayan, MBBS, PhD, FRACS*†‡

Background: Cancer patients often require radiotherapy (RTx) to enhance their survival. Unfortunately, RTx also damages nearby healthy non-cancer tissues, leading to progressive fibrotic soft-tissue injury, consisting of pain, contracture, tissue-breakdown, infection, and lymphoedema. Mechanisms underlying the clinically observed ability of fat grafting to ameliorate some of these effects, however, are poorly understood. It was hypothesized that RTx significantly alters fibroblast cell function and the paracrine secretome of adipose-derived stem cells (ADSC) may mitigate these changes.

Methods: To investigate cellular changes resulting in the fibrotic side-effects of RTx, cultured normal human dermal fibroblasts (NHDF) were irradiated (10Gy), then studied using functional assays that reflect key fibroblast functions, and compared with unirradiated controls. RNA-Seq and targeted microarrays (with specific examination of TGFβ) were performed to elucidate altered gene pathways. Finally, conditioned-media from ADSC was used to treat irradiated fibroblasts and model fat graft surgery.

Results: RTx altered NHDF morphology, with cellular functional changes reflecting transition into a more invasive phenotype: increased migration, adhesion, contractility, and disordered invasion. Changes in genes regulating collagen and MMP homeostasis and cell-cycle progression were also detected. However, TGFβ was not identified as a key intracellular regulator of the fibroblast response. Finally, treatment with ADSC-conditioned media reversed the RTx-induced hypermigratory state of NHDF.

Conclusions: Our findings regarding cellular and molecular changes in irradiated fibroblasts help explain clinical manifestations of debilitating RTx-induced fibrosis. ADSC-secretome-mediated reversal indicated that these constituents may be used to combat the devastating side-effects of excessive unwanted fibrosis in RTx and other human fibrotic diseases. *(Plast Reconstr Surg Glob Open 2020;8:e2706; doi: 10.1097/GOX.0000000000002706; Published online 24 March 2020.)*

*From the *Regenerative Surgery and Lymphatics Department, O'Brien Institute, St. Vincent's Institute, Fitzroy, Victoria, Australia; †Department of Plastic Surgery, St. Vincent's Hospital, Fitzroy, Victoria, Australia; ‡Department of Health Science and Exercise Science Bioengineering Lab, Australian Catholic University and O'Brien Institute Tissue Engineering Centre, Regenerative Surgery Group (AORTEC), Fitzroy Street, Fitzroy, Victoria, Australia; §Skin Bioengineering Laboratory, Victorian Adult Burns Service, The Alfred Hospital, Victoria, Australia; ¶Department of Surgery, The University of Melbourne, The Royal Melbourne Hospital, Victoria, Australia; and ‖Epigenetics and Development Division, The Walter and Eliza Hall Institute of Medical Research, Parkville, Victoria, Australia.*

Received for publication September 20, 2019; accepted January 27, 2020.

Copyright © 2020 The Authors. Published by Wolters Kluwer Health, Inc. on behalf of The American Society of Plastic Surgeons. All rights reserved.This is an open-access article distributed under the terms of the Creative Commons Attribution-Non Commercial-No Derivatives License 4.0 (CCBY-NC-ND), where it is permissible to download and share the work provided it is properly cited. The work cannot be changed in any way or used commercially without permission from the journal.

DOI: 0.1097/GOX.0000000000002706

INTRODUCTION

Over half of all patients diagnosed with solid malignancies require radiotherapy (RTx). Despite significantly enhancing survival, RTx damages healthy native tissues, inducing progressive soft-tissue injury that may intensify

Disclosures: *The O'Brien Institute acknowledges funding support from the Victorian State Government's Department of Innovation, Industry and Regional Development's Operational Infrastructure Support Program, Royal Australasian College of Surgeons Foundation for Surgery and Tour de Cure Scholarship, The Wicking Foundation, ACU AORTEC, Stafford Fox Medical Research Foundation, Australasian Foundation for Plastic Surgery, LEW Carty Charitable Fund, Joe White Bequest and the Viertel Charitable Foundation. None of the authors has a financial interest in any of the products, devices, or drugs mentioned in this manuscript.*

Related Digital Media are available in the full-text version of the article on www.PRSGlobalOpen.com.

years later, characterized by pain, contracture, tissue breakdown, recurrent infection, and lymphoedema.[1]

On a cellular/molecular level, RTx-injury has been characterized as fibro-proliferative[1]—fibroblasts deposit collagen/other ECM products, generating a scar "patch" within injured areas, rather than exactly regenerating original tissue.[2] This "abnormal" tissue may itself lead to clinical problems (Fig. 1A), ranging from scarring, contracture (eg, of breast prosthetic capsule or joint),[3] restricted movement, and poor healing (chronic ulceration or spontaneous wound breakdown) that may expose important underlying structures (Fig. 1B).[4] Such wounds require specialized dressing and antimicrobial regimes and, often, surgery. Due to the paucity of locoregional options, these wounds present difficult plastic surgical challenges, frequently requiring more complex reconstructive measures, such as free flaps[5,6] (Fig. 1C).

Therefore, methods to reduce RTx-induced fibrosis would improve the functional integrity of irradiated tissues and ameliorate unwanted sequalae, thus improving clinical outcome. A set of in vitro assays was designed to characterize fibrotic and other effects of external-beam gamma radiation on normal human dermal fibroblast (NHDF) cellular functions.[7] To identify novel therapeutic candidates by which to reverse RTx-induced fibrosis, cellular behavior alterations were cross-referenced with molecular and genetic changes thus detected.

Clinically, fat grafting for cosmetic or traumatic contour correction and to scarred, contracted tissue, is gaining popularity in plastic surgery.[8,9] The application of fat grafting for these indications in breast and head and neck cancer patients resulted in serendipitous observations that fat grafts improved RTx-induced capsular contracture, chronic ulceration, and vocal cord damage.[10–19] It highlighted the regenerative potential of fat and the need for scientific evaluation of underlying mechanisms.

The clinical benefits of fat grafting are postulated to be due to regenerative properties of multi-potent adipose-derived stem cells (ADSCs) within fat and their unique paracrine secretome.[13,20] Clinical effects occur through adipogenesis, angiogenesis, and lymphangiogenesis[21]; and/or induction or modulation of inflammatory, immune and reactive oxygen species-mediated processes and cell recruitment.[22,23] However, despite established clinical application of fat grafting and suggested *theoretical* regenerative mechanisms, accurate molecular understanding of what drives ADSC-mediated RTx-injury reversal remains poor.[9,24] Haubner's study demonstrated reduced upregulation of inflammatory cytokines IL-6, FGF, ICAM-1, and VCAM1 in irradiated blood endothelial cells after coculture with ADSCs.[25] Chang et al. showed improved intestinal re-epithelialization and survival after irradiation and intraperitoneal ADSC treatment.[26] Sultan et al. and Huang et al. showed dermal improvement and changes to collagen-based scar indices and fibrosis markers (Smad-3) in fat-grafted irradiated animal skin models.[27,28]

Using in vitro models, we sought to establish baseline RTx effects on NHDF cellular function and identify associated molecular changes underpinning them, which we hypothesized to be significantly altered in comparison to un-irradiated NHDF. We then examined the regenerative effect of ADSCs, on the most markedly altered irradiated NHDF function, in order elucidate mechanisms by which fat grafting may improve the aftereffects of cancer treatment.[10–19] In particular, the molecular candidates identified will provide clues toward developing novel therapeutic approaches in the setting of RTx-induced soft-tissue injury, especially in ameliorating RTx-induced fibrosis.

METHODS

Cell Culture and Irradiation

Primary proliferating NHDF (PromoCell Germany) cultures were established and incubated (37°C, 5% CO_2) in flasks (CELLSTAR, Germany) in DMEM [4.5 g/L Glucose with Glutamine (Lonza, Switzerland)], 10% FCS (SAFC Biosciences; Sigma Aldrich, Missouri), and antibiotics and not used beyond passage 4. Briefly, NIH3T3-*pCAGA*$_{12}$-*luc* cells were generated using methods described by Dennler et al, 1998.[29] NHDFs received 10Gy [Gammacell

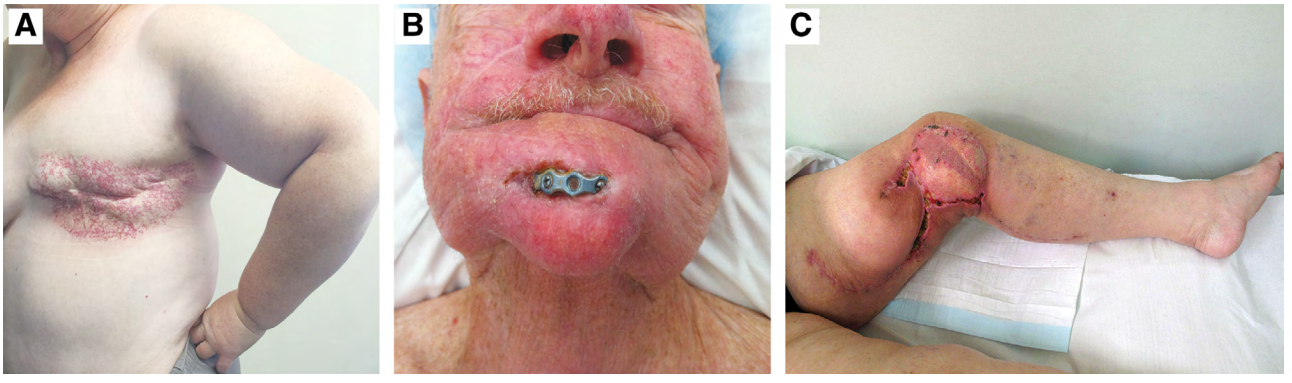

Fig. 1. Clinical manifestations of RTx-induced soft tissue injury. Clinical photographs demonstrating the spectrum of complications resulting from RTx-induced soft tissue injury to normal tissues. A, Adjuvant RTx for control of lymph node involvement of cancers from the breast or chest wall resulting in severe scarring, telangiectasia skin change and fibrosis, which can significantly impair the mobility of soft tissue the upper limb due to axillary contractures. B, The integrity and compliance of irradiated tissues is compromised, resulting in wound break down and exposure of underlying structures such as bone or metal reconstruction plates. C, Demonstrates significant issues with wound healing, even in situations where healthy, un-irradiated tissue (flap) has been transferred from a distant site of the body to the irradiated field.

40 Irradiator (Best Theratronics, Canada), Bio-resources Centre, St. Vincent's Hospital, Victoria, Australia], or 0Gy sham treatment (**see document, Supplemental Digital Content 1**, which displays invitro irradiation dose design and optimization. http://links.lww.com/PRSGO/B333).

ADSC Isolation Generation of ADSC-Conditioned Media

ADSCs were isolated using established protocols[30] from excess fresh adipose/lipoaspirate tissues of healthy patients undergoing surgery at St. Vincent's Hospital (Victoria, Australia) (HREC 52/03). After digestion with collagenase, ADSC were cultured to 80%–90% confluence, then fresh DMEM was placed in each culture flask for conditioning. At 72 hours, ADSC-conditioned media (CM) was aspirated, centrifuged, and filtered [0.22 μm Millex-GV Syringe Filter Unit (EMD Millipore, Germany)] and used to determine the paracrine regenerative capacity of ADSC on irradiated NHDF. For media composition, see Supplemental Digital Content 2. (**See table, Supplemental Digital Content 2**, which displays media solution composition for in vitro assays, http://links.lww.com/PRSGO/B334.)

In Vitro Functional Assays

Forty-eight hours later, luminescence-based assays were used to assess NHDF proliferation and apoptosis with CellTiter-Glo Cell Viability (Promega; Fitchburg, Wisc.) and Caspase-Glo 3/7 Assays (Promega), respectively, as per manufacturer's instructions. 5,000–20,000 NHDF 3D spheroids were formed using 20% methylcellulose in 80% DMEM solution in U-bottom 96-well plates (BD Falcon, New Jersey).

Scratch migration assays were conducted using NHDFs in pre-coated [10 μg/mL Human Fibronectin (Sigma Aldrich, Australia)], subjected to 10Gy or 0Gy treatment. NHDFs were serum-starved before being scratched at 48 h posttreatment then washed and replenished with control/experimental media and imaged at 0 and 48 h [Olympus IX71 Inverted Microscope; Olympus, Tokyo, Japan]. Scratch areas were quantified as % gap closure, calculated by creating a "wound mask" (ImageJ; NIH, Bethesda, Maryland) (Fig. 3).

RTx effects on NHDF outgrowth/invasion were assessed by seeding 5,000 NHDFs into 50 μl of Cultrex invasion matrix (Trevigen, Gaithersburg, Maryland) in a spheroid-forming plate. Images of spheroid morphology and area of cellular outgrowth were captured on brightfield microscopy for 11 days by observers blinded to the irradiation status, then quantified using ImageJ (LVAP plugin).[31]

Cell adhesion assays were conducted on 0–5 ng/ml concentration collagen I-coated 96-well plates (Sigma Aldrich, Australia). NHDFs were blocked (3% BSA), trypsinized (48 h after RTx), and suspended in normal media (0.1% BSA). NHDFs were fixed (methanol), stained with crystal violet ($C_{25}N_3H_{30}Cl$), and washed (dH_2O) before 0.1 M sodium citrate solution was added for dye extraction quantification (540 nm absorbance) by microplate spectrophotometry (Benchmark Plus; Biorad, Calif.).

0Gy and 10Gy NHDFs were seeded (500,000 cells/well) into 200 μl of 70% collagen-1, 10% 10× PBS (Lonza; Basel, Switzerland), 20% $NaHCO_3$ (11.76 mg/ml) (Sigma Aldrich, Australia) gel. Forty-eight hours later, gels were released and allowed to float in media (24 h). Fold change differences in collagen gel area were quantified in ImageJ to assess contracture.

Organotypic Culture Model

De-epidermized dermis (DED) was generated from excess patient skin discarded after elective surgery (Alfred Hospital, Victoria, Australia) (HREC 269/16). This involved sterilization, de-epidermization, and accellularization as described previously in Livesey et al.[32] To create organotypic culture models, DED was cut into $1 \times 1\,cm^2$ pieces and used as a seeding matrix. NHDFs were seeded after irradiation at 0.5×10^6 cell density in 50 μl of DMEM, using ring constructs within culture plates. Samples were fixed at 48 hours (4% PFA then 10% formalin) and organotypic culture tissues embedded in paraffin blocks and H&E stained. The area covered by NHDF growth and invasion was quantified in ImageJ by an observer blinded to irradiation status.

mRNA Extraction, Microarray, and Next Generation Gene Sequencing

mRNA was extracted from NHDFs 4 hours after RTx or control treatment using Qiazol (QIAGEN, Germany), and purified with DNase and RNEasy Plus Universal Kit (QIAGEN, Germany). mRNA extracts underwent Next generation gene sequencing (100 base pair single end) on an HiSeq machine (Illumina; Best Theratronics, ON, Canada). Reads from each sample were mapped to the hg19 genome and differential expression was assessed via linear models using the Rsubread, edgeR, and limma software.[33–35] The voom method was applied to deal with observational-level heteroscedasticity and to summarize expression values per gene across replicate samples.[36] Next, empirical Bayes' shrinkage[37] was applied to moderate the standard errors of the log-fold changes estimated between the 10Gy and 0Gy samples. A false discovery rate cutoff of <0.05 was used to determine differentially expressed genes.[38]

To interrogate post-RTx mRNA alterations in Human ECM-related genes, PCR mini-array analysis was conducted using a custom mini-array [384-well custom RT² Profiler PCR Array—84 genes (QIAGEN, Germany)]. 10Gy RNA expression was normalized to 0Gy expression at 48 hours represented as a fold change based on the $\Delta\Delta C_T$ method with normalization of the raw data to housekeeping genes.

Luciferase Assays: Quantifying Active TGF-β Concentrations in Conditioned Media

NIH3T3-*pCAGA$_{12}$-luc* cells (5×10^4/well) were seeded in 96-well plates overnight and then treated with a range of TGF-β concentrations to obtain a standard curve. For total TGF-β levels, supernatant was heat-activated (90°C, 10 min),[35] before addition to the NIH3T3-*pCAGA$_{12}$-luc* cells. After 24 hours, NIH3T3-*pCAGA$_{12}$-luc* cells were lysed and assessed for luciferase activity using the Luciferase Reporter Assay Kit (Promega) following the manufacturer's instructions. Sample values were interpolated as per standard curves to quantify secreted TGFβ levels (active and latent forms[39]).

Statistical Analysis

Statistical analysis was conducted using a Student's *t* test or 1-way ANOVA, with or without multiple group comparisons, where indicated. *P* value <0.05 was considered

significant. All experiments n ≥ 3. (GraphPad Prism 6.0; GraphPad, San Diego, Calif.).

RESULTS

RTx Alters Key In Vitro Cellular Functions of NHDFs

Cell Morphology. Morphological differences between 0Gy and 10Gy NHDFs were seen in culture. Irradiated cells displayed elongated, enlarged morphology. To quantify this observation in 3D, spheroids were formed in 5,000–20,000 cells/spheroid variations. 10Gy spheroids displayed significantly increased area compared with 0Gy controls, across all variations (Fig. 2A). 10Gy groups demonstrated average area fold increases of 1.49 ± 0.21 (5,000 cells/spheroid), 1.27 ± 0.19 (10,000 cells/spheroid), and 1.74 ± 0.17 (20,000 cells/spheroid) ($P < 0.01$ for all).

Proliferation and Apoptosis

10Gy NHDF proliferation was reduced compared with 0Gy controls, 48 hours after RTx (Fig. 2B), with a mean difference of 13.6 ± 3.7% ($P < 0.05$). Meanwhile, irradiated NHDFs did not demonstrate significantly increased rates of apoptosis compared with 0Gy controls.

Adhesion and Contraction

Quantification of crystal violet staining of adherent NHDFs demonstrated that 10Gy samples were more adherent than 0Gy counterparts across various collagen-I concentrations, with the greatest difference on 5 ng/ml collagen-I [10Gy NHDFs were 49 ± 15% ($P < 0.05$) more adherent than 0Gy NHDFs (Fig. 2C)]. In terms of gel contraction,

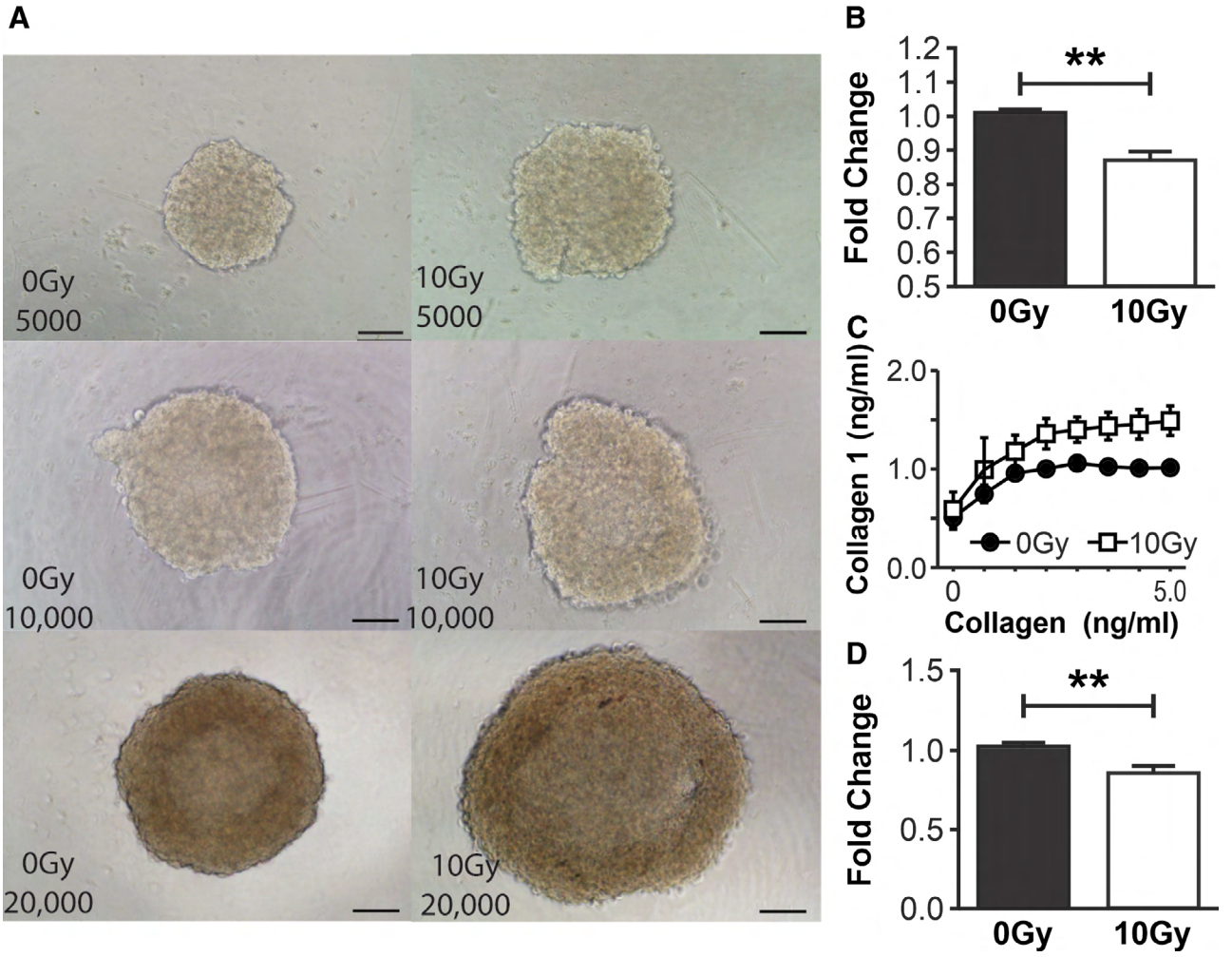

Fig. 2. RTx alters the cellular functions of NHDF. A, NHDF spheroids imaged using bright-field microscopy (×10 objective) in the following variations: 0Gy 5,000 cells/spheroid, 10Gy 5,000 cells/spheroid, 0Gy 10,000 cells/spheroid, 10Gy 10,000 cells/spheroid, 0Gy 20,000 cells/spheroid, 10Gy 20,000 cells/spheroid validating the morphological increase in 10Gy NHDF size with the demonstrable increase in 10Gy spheroids size compared with the relevant 0Gy cells/spheroid control. B, Quantification of proliferation of NHDF demonstrates a significant reduction in proliferation after 10Gy irradiation compared with 0Gy controls at 48 h. C, Quantification of adherent 0Gy and 10Gy NHDF by solubilization of crystal violet and spectrophotometric analysis at 540 nm demonstrates a global increase in the number of adherent 10Gy NHDF at all collagen-I concentrations (0–5 ng/ml) compared with 0Gy controls. Fixed collagen-I gels were released circumferentially from well edges 48 h after seeding with 0Gy NHDF and 10Gy NHDF, allowed to float in media and contract over 24 h. D, Quantification of gel areas demonstrated a reduction in 10Gy NHDF collagen-I gel area, (reflecting increased contractile ability) compared with 0Gy NHDF gels. Scale bars (A) 100μm. (**P value < 0.01). Error bars represent SEM, n ≥ 3 for all experiments.

10Gy NHDF collagen-I gels demonstrated 16.9 ± 6.1% ($P < 0.05$) greater contractility compared with 0Gy NHDF counterparts (Fig. 2D). Increased contraction observed after RTx was further investigated by αSMA immunohistochemical staining to detect potentially contractile cells.[7,40] Microscopic analysis demonstrated that in 0Gy NHDF samples, minimal αSMA was seen in the cytoplasm, and the majority of the signal was located at the cell periphery. Conversely, 10Gy NHDFs demonstrated increased αSMA expression, which was more uniformly distributed throughout the cell cytoplasm. (**See figure, Supplemental Digital Content 3,** which displays how radiotherapy alters the distribution of αSMA expression in NHDF in vitro and increases the perivascular expression in irradiated tissue samples, http://links.lww.com/PRSGO/B335.) Human skin tissue samples demonstrated increased dermal and perivascular staining in irradiated tissues in comparison to patient matched normal skin controls. (**See figure, Supplemental Digital Content 3,** http://links.lww.com/PRSGO/B335.)

Migration and Invasion

Scratch assays demonstrated increased migration in 10Gy NHDFs, compared with 0Gy controls, from 0 hours (Fig. 3A) onwards. At 48 hours, 0Gy (Fig. 3B) and 10Gy

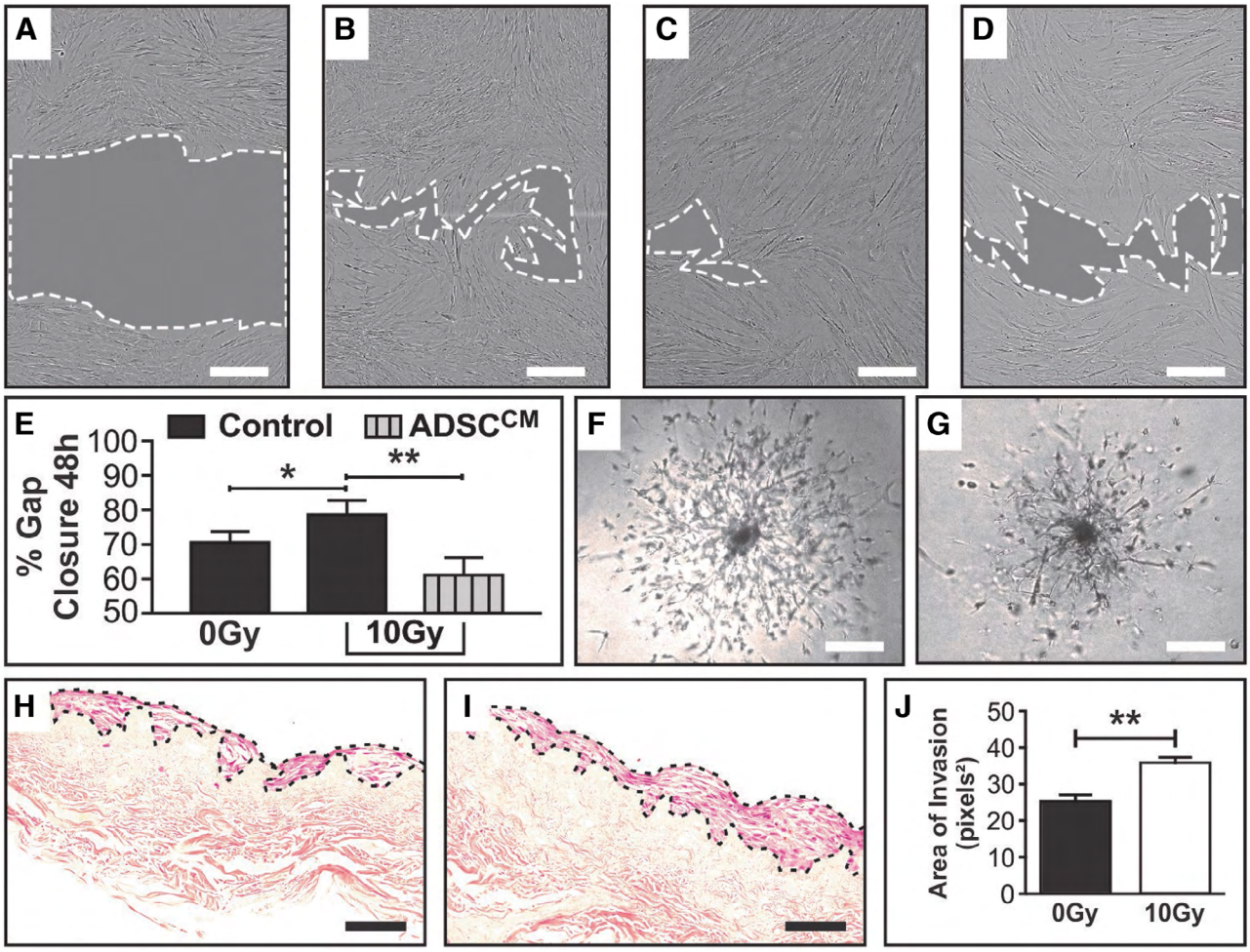

Fig. 3. RTx increases the migratory capacity of NHDF, a change that is reversed with the addition of ADSC^{CM}. ×10 objective bright field imaging of NHDF was taken at 0 and 48 h post creation of the scratch wound on a confluent mono-layer of proliferating cells. A, Representative image of NHDF scratch wound area at 0 h, (B) 0Gy NHDF in control media (complete DMEM) scratch wound area at 48 h, (C) 10Gy NHDF in control media (complete DMEM) scratch wound area at 48 h, (D) 10Gy NHDF in ADSC^{CM} scratch wound area at 48 h. (E) Quantification and analyses of the % gap closure at 48 h compared with 0 h controls demonstrating differences resulting from RTx injury and treatment with ADSC^{CM} in a model of fat grafting. % Gap closure between 0Gy (B) and 10Gy (C) NHDF scratch wound areas at the 48 h end-point graphically demonstrates the unexpected increase in migration of 10Gy NHDF, while addition of ADSC^{CM} to 10Gy NHDF (D) mitigated this hypermigratory state. F, 0Gy NHDF cell outgrowth captured at Day 11 demonstrating a symmetrical pattern of invasion migrating from a central core of cells. G, 10Gy NHDF cell outgrowth captured at Day 11 demonstrating asymmetrical and disordered sprouting from a denser central core of cells, captured at ×4 objective using bright field microscopy. H, 0Gy NHDF and (I) 10Gy NHDF on DED matrix (transverse section ×20 objective), with (J) quantification of the NHDF cell layer area demonstrating a significantly thicker layer of cells with a broader front of invasion in the 10Gy irradiated group. In (A–D), scale bar 300μm, dotted white line represents periphery of scratch wound and gray shaded area represents scratch wound area. Scale bars in F–G 300 μm and H–I 50 μm (*P value <0.05; **P value <0.01). Error bars represent SEM, n ≥ 3 for all experiments.

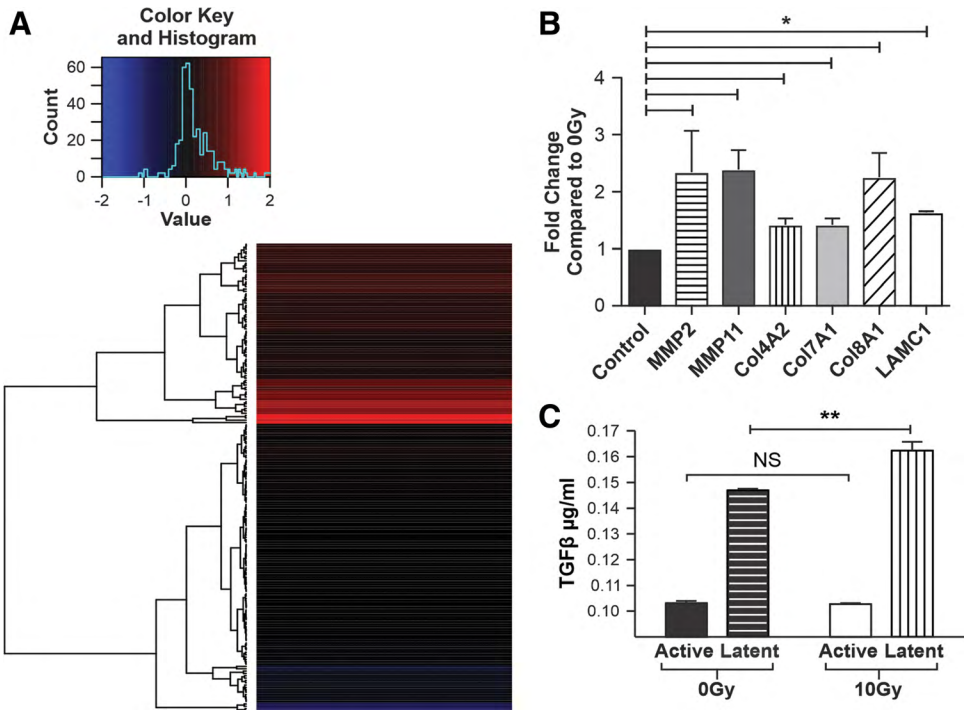

Fig. 4. RTx alters the molecular expression of extracellular matrix and p53 pathway genes without significant change in active TGFβ. A, Heat map of genes activated in the p53 pathway post irradiation of NHDF. B, A graph depicting the statistically significant ECM genes upregulated by RTx injury of NHDF at the 48 h time point compared with 0Gy controls. C, A graph demonstrating the effects of RTx on secretion of TGFβ in both active and latent states. Activated levels of TGFβ did not differ significantly between 0Gy and 10Gy groups, while latent levels only demonstrated a small significant increase in 10Gy compared with 0Gy NHDF controls. *P < 0.05, **P value < 0.01, NS = not significant). Error bars represent SEM, n ≥ 3 for all experiments.

(Fig. 3C)NHDFs exhibited 71 ± 2.8% and 79 ± 3.8% gap closure, respectively, representing a difference of 8 ± 2.9% [P < 0.05 (Fig. 3E)]. In 3D spheroid assays, 0Gy NHDFs demonstrated symmetrical outgrowth from spheroids (Fig. 3F). In contrast, 10Gy NHDFs exhibited highly disordered outgrowth from more densely adherent cell masses that became increasingly asymmetrical and fragmented over the next 11 days (Fig. 3G). 3D organotypic culture invasion modeling comparing 0Gy NHDF (Fig. 3H) with 10Gy NHDF (Fig. 3I) demonstrated that irradiated cells were "heaped-up" in a thicker layers with a broader front of dermal invasion. This thickening, quantified using ImageJ on ×20 objective images as area covered by NHDFs (Fig. 3H,I), demonstrated an average thickness of 36.2 ± 1.3 pixels^2 in 10Gy groups, compared with 25.5 ± 1.7 pixels^2 in 0Gy samples (P< 0.01) (Fig. 3J).

RTx Significantly Alters the Molecular Expression Profile of NHDFs

RNA-Seq of NHDFs 4 hours after RTx demonstrated significant differential expression between 10Gy and 0Gy NHDFs, in 86 genes. (**See figure, Supplemental Digital Content 4,** which displays Next Generation Sequencing data demonstrating significantly altered RNA expression in irradiated NHDF compared with controls, http://links.lww.com/PRSGO/B336.) Among the top 10 genes altered in irradiated NHDFs, important genes relating to the abnormal functional profile observed, above, included CDKN1A, GADD45A, TP53INP1, MDM2. These altered genes play key roles in cell cycle regulation/arrest or DNA damage response and repair, by exerting antioxidant, antiproliferative, and pro-apoptotic effects.[41] Analysis demonstrated significant gene enrichment in the p53 signaling pathway (Fig. 4A). Significant enrichment of the TGFβ1-related signaling pathways, which have been thought to exert a pivotal influence on RTx-treated tissue, was not detected (data not shown).[42]

Forty-eight hours after 10Gy and 0Gy RTx, custom microarray analysis was performed to identify key genes altered at the time point at which the cell-function assays (above) were conducted. Six key ECM genes were found to be significantly differentially upregulated in 10Gy samples (Fig. 4B). Specifically, MMP family subtypes 2 and 11 showed 2.07- and 2.31-fold increases, respectively; while collagens 4A2, 7A1, and 8A1 demonstrated 1.41-, 1.51-, and 2.14-fold increases, respectively, in response to 10Gy RTx. Laminin C1 demonstrated a 1.64-fold increase (Fig. 4B).

To further investigate the TGFβ axis, specific analysis of both latent and active forms of TGFβ was performed. In contrast to traditional dogma regarding TGFβ, mRNA for TGFβ was unaltered in irradiated samples. (**See table, Supplemental Digital Content 2,** which displays media solution composition for in vitro assays, http://links.lww.com/PRSGO/B334; Fig. 2.) To uncover whether this finding

was due to differential changes in either the latent or active form, processing to allow activation of latent TGFβ was also conducted. As was the case in mRNA analysis, no significant difference was seen between active TGFβ levels secreted by NHDFs following either 10Gy or 0Gy treatment at the protein level. While, 0Gy samples were found to secrete 147 ± 0.61 ng/ml of latent TGFβ, 10Gy samples secreted only mildly increased levels of latent TGFβ 162 ± 0.35ng/ml ($P < 0.05$) (Fig. 4C).

ADSC^{CM} Reverses NHDF Hyper-migration in RTx-injury

To validate observations regarding fat grafting made in clinical practice, ADSC^{CM} was added to populations of both irradiated and control NHDFs. While ADSC^{CM} did not significantly alter gap closure at 48 hours in 0Gy NHDFs, ADSC^{CM}-treated 10Gy NHDFs exhibited significantly diminished gap closure 61.4 ± 8.1% (Fig. 3D), compared with untreated 10Gy NHDF counterparts (79 ± 6.6%) (Fig. 3C). This represented a 17.5% ($P < 0.01$) reduction in overall migration of 10Gy NHDFs after ADSC^{CM} treatment (Fig. 3E).

DISCUSSION

To elucidate the fibrotic influences of RTx on soft-tissues and potential avenues for reversal, RTx effects on NHDF (the cell-type associated with tissues fibrosis) were studied. RNA-seq of RTx-treated NHDFs was performed, before ADSC-mediated treatment was modeled. Taking our cell function and molecular assays together, our data revealed novel findings that challenge traditionally held concepts of RTx exerting suppressive influences on NHDFs.

We found that reduced NHDF cell-survival was chiefly due to impaired proliferative capacity, rather than increased apoptosis. This balance was mediated by RTx-induced cellular senescence, as cells remained halted in post-mitotic phase or terminally differentiated (unable to functionally contribute to regenerative wound-healing[43,44]). Defining features supporting the concept of RTx promoting cell senescence—such as cell flattening, increased size/swelling, and reduced proliferative potential—were observed in irradiated NHDFs.[45,46] Senescence leads to telomere shortening and p53-dependent DNA damage response pathway activation, which facilitate cell cycle arrest.[47] We showed significant RTx-induced transcriptional alteration, with mRNA upregulation of several anti-proliferation genes (CDKN1A, GADD45A, TP53INP1, MDM2), in keeping with cell cycle arrest.[41]

Counter-intuitively, we observed *increased*, disordered NHDF migration following RTx-injury in 2D (scratch-wound) and 3D (spheroid and organotypic invasion) assays. While increased migration may seem beneficial for healing,[48] dysregulated, random, hypermigration in sublethally injured cells actually represents functional impairment and contributes to increased contractility despite a reduction in proliferation. This hypermigratory behavior helps explain propagation of RTx-damage beyond targeted RTx fields, as seen in "Radiation-Induced Bystander Effect."[49] Normally, migrating cell fronts necessitate coordinated sequential cell assembly, ECM breakdown, and cytoskeletal re-organization.[50] Instead, post-RTx migratory patterns showed spatially disordered, haphazard propagation, and outgrowth from denser cores of adherent NHDFs in 3D spheroid constructs, with tendencies toward greater contractility (Fig. 2C). Meanwhile, in 3D organotypic culture, irradiated NHDFs demonstrated thickened, more confluent cellular layers on DED matrix (Fig. 3I). We found that irradiated NHDF-mediated ECM alterations lead to upregulation of collagen subtypes 4A2, 7A1, 8A1, and of Laminin1C, enhancing our understanding of classically reported collagens I and III upregulation.[51–54] Impaired ECM remodeling is characteristic of many fibrotic pathologies—ECM provides structural support but is also dynamic and can itself regulate cell behavior via signaling modulation.[55] For example, Laminin and Collagen IV are integral components of the basement-membrane zone (BMZ), a key cell behavioral regulator.[56] Upregulation of collagen IV and laminin gene expression have 2 key effects: first, BMZ hypertrophy in skin and vascular structures may impair tissue compliance and reduce angiogenic and lymphangiogenic (integral processes in healing) capacity. Second, BMZ thickening may bolster antitumor benefits of RTx, thickening substrate barriers through which residual/recurrent cancer cells must invade to spread—thus "confining" metastatic cells. Collagen VII is a network-forming collagen,[57] interacting with laminin, collagen IV, and dermal collagen I to provide connections between epidermal and dermal compartments.[54] The effects of excess collagen VII are not well described, while collagen VII deficiency underpins skin desquamation/fibrosis in epidermolysis bullosa.[57] Col VIIA2 upregulation could, therefore, account for increased NHDF anchoring or adhesion on collagen I matrices. Our study also demonstrated significant RTx-induced upregulation of expression of proteolytic genes, MMP-2, and -11 in NHDFs. MMP-2-mediated fibronectin degradation may facilitate NHDF hypermigratory/sprouting behavior after RTx; however, it may also destabilize dermal structural integrity, especially when challenged by trauma or re-operation in irradiated fields.[58]

Our analysis of RTx-effects on TGFβ expression/secretion by NHDFs also contradicted long-standing dogma implicating TGFβ-signaling in RTx-induced soft-tissue fibrosis.[42,59] While RTx caused mildly increased *latent* TGFβ expression in NHDFs, active TGFβ levels were unchanged. This suggests that canonical TGFβ/Smad3-mediated signaling and downstream transcription[60,61] may not play a role in RTx-induced NHDF alterations in vitro or, therefore, be useful in combating fibroblast-driven fibrosis.

To investigate the role of fat grafting and explore therapeutic avenues by which to reduce RTx-induced fibrosis, putative ADSC regenerative properties were modeled. ADSC^{CM} added to irradiated/control NHDFs reversed hypermigration in 10Gy groups, suggesting that factors in the ADSC secretome can salvage RTX-injured NHDFs. Introducing fat grafts into a pre-irradiated tissue bed may, therefore, restrict the spread of RTX-injury and fibrosis. These novel results explain clinical observations of softening and reduced fibrosis after fat grafting.[13]

CONCLUSIONS

Collectively, these data reveal key mechanisms by which irradiating normal tissues leads to poor wound healing and unwanted progressive, maladaptive fibrosis. RTx causes abnormal morphology, behavioral, and synthetic functional changes in NHDFs, dysregulating important signaling pathways and homeostatic functions. Sublethally, RTx-injured NHDFs were characterized by a hypoproliferative but more exuberant hypermigratory, invasive, adherent, and contractile phenotype. Interestingly, NHDF "senescence" represented transition to a less apoptotic state.

ADSC^{CM}-mediated reversal of the hypermigratory behavior enhances our understanding of cellular/molecular mechanisms underlying RTx-induced fibrosis, therapeutic reversal of NHDF dysfunction and the regenerative capacity of fat grafts, ADSCs, or their secretome/constituents. By repairing damaged pathways, we hope to reduce the debilitating disease burden and chronic consequences of excessive, unwanted fibrosis in cancer survivors.

Lipi Shukla
O'Brien Institute
St. Vincent's Hospital
42 Fitzroy Street
Fitzroy, Melbourne, VIC 3065, Australia
E-mail: lipi.shukla@gmail.com

ACKNOWLEDGMENTS

The authors thank Janna Taylor for preparation of figure and table layouts, Jason Palmer for technical assistance with immunohistochemical staining, Nicole Harris for facilitating cell transfer to Melbourne University Lab, and Ilia Banakh for processing specimen in the Bioengineering Laboratory.

REFERENCES

1. Rodemann HP, Bamberg M. Cellular basis of radiation-induced fibrosis. *Radiother Oncol.* 1995;35:83–90.
2. Korwar V, Skillman J, Matey P. Skin reducing mastectomy and immediate reconstruction: the effect of radiotherapy on complications and patient reported outcomes. *Eur J Surg Oncol.* 2014;40:442–448.
3. Fischer JP, Basta MN, Shubinets V, et al. A systematic meta-analysis of prosthetic-based breast reconstruction in irradiated fields with or without autologous muscle flap coverage. *Ann Plast Surg.* 2014;77:129–134.
4. Kim JH, Jenrow KA, Brown SL. Mechanisms of radiation-induced normal tissue toxicity and implications for future clinical trials. *Radiat Oncol J.* 2014;32:103–115.
5. Weintraub NL, Jones WK, Manka D. Understanding radiation-induced vascular disease. *J Am Coll Cardiol.* 2010;55:1237–1239.
6. Dormand EL, Banwell PE, Goodacre TE. Radiotherapy and wound healing. *Int Wound J.* 2005;2:112–127.
7. McAnulty RJ. Fibroblasts and myofibroblasts: their source, function and role in disease. *Int J Biochem Cell Biol.* 2007;39:666–671.
8. Zuk PA, Zhu M, Mizuno H, et al. Multilineage cells from human adipose tissue: implications for cell-based therapies. *Tissue Eng.* 2001;7:211–228.
9. Phinney DG, Prockop DJ. Concise review: mesenchymal stem/multipotent stromal cells: the state of transdifferentiation and modes of tissue repair–current views. *Stem Cells.* 2007;25:2896–2902.
10. Poglio S, Galvani S, Bour S, et al. Adipose tissue sensitivity to radiation exposure. *Am J Pathol.* 2009;174:44–53.
11. Serra-Renom JM, Muñoz-Olmo JL, Serra-Mestre JM. Fat grafting in postmastectomy breast reconstruction with expanders and prostheses in patients who have received radiotherapy: formation of new subcutaneous tissue. *Plast Reconstr Surg.* 2010;125:12–18.
12. Coleman SR. Structural fat grafts: the ideal filler? *Clin Plast Surg.* 2001;28:111–119.
13. Tabit CJ, Slack GC, Fan K, et al. Fat grafting versus adipose-derived stem cell therapy: distinguishing indications, techniques, and outcomes. *Aesthetic Plast Surg.* 2012;36:704–713.
14. Rigotti G, Marchi A, Galiè M, et al. Clinical treatment of radiotherapy tissue damage by lipoaspirate transplant: a healing process mediated by adipose-derived adult stem cells. *Plast Reconstr Surg.* 2007;119:1409–1422; discussion 1423.
15. Ross RJ, Shayan R, Mutimer KL, et al. Autologous fat grafting: current state of the art and critical review. *Ann Plast Surg.* 2014;73:352–357.
16. Mizuno H, Hyakusoku H. Fat grafting to the breast and adipose-derived stem cells: recent scientific consensus and controversy. *Aesthet Surg J.* 2010;30:381–387.
17. Akita S, Yoshimoto H, Ohtsuru A, et al. Autologous adipose-derived regenerative cells are effective for chronic intractable radiation injuries. *Radiat Prot Dosimetry.* 2012;151:656–660.
18. Suga H, Eto H, Aoi N, et al. Adipose tissue remodeling under ischemia: death of adipocytes and activation of stem/progenitor cells. *Plast Reconstr Surg.* 2010;126:1911–1923.
19. von Heimburg D, Hemmrich K, Zachariah S, et al. Oxygen consumption in undifferentiated versus differentiated adipogenic mesenchymal precursor cells. *Respir Physiol Neurobiol.* 2005;146:107–116.
20. Thanik VD, Chang CC, Lerman OZ, et al. A murine model for studying diffusely injected human fat. *Plast Reconstr Surg.* 2009;124:74–81.
21. Shukla L, Morrison WA, Shayan R. Adipose-derived stem cells in radiotherapy injury: a new frontier. *Front Surg.* 2015;2:1.
22. Zhu M, Zhou Z, Chen Y, et al. Supplementation of fat grafts with adipose-derived regenerative cells improves long-term graft retention. *Ann Plast Surg.* 2010;64:222–228.
23. Butala P, Sultan SM, Davidson EH, et al. Augmentation of fat graft survival with progenitor cell mobilization. *Plast Reconstr Surg.* 2010;125(Supplement):12.
24. Haubner F, Eto H, Leyh M, et al. The fate of adipocytes after nonvascularized fat grafting: evidence of early death and replacement of adipocytes. *Plast Reconstr Surg.* 2012;129:1081–1092.
25. Haubner F, Leyh M, Ohmann E, et al. Effects of external radiation in a co-culture model of endothelial cells and adipose-derived stem cells. *Radiat Oncol.* 2013;8:66.
26. Chang P, Qu Y, Liu Y, et al. Multi-therapeutic effects of human adipose-derived mesenchymal stem cells on radiation-induced intestinal injury. *Cell Death Dis.* 2013;4:e685.
27. Sultan SM, Stern CS, Allen RJ Jr, et al. Human fat grafting alleviates radiation skin damage in a murine model. *Plast Reconstr Surg.* 2011;128:363–372.
28. Huang SP, Huang CH, Shyu JF, et al. Promotion of wound healing using adipose-derived stem cells in radiation ulcer of a rat model. *J Biomed Sci.* 2013;20:51.
29. Dennler S, Itoh S, Vivien D, et al. Direct binding of smad3 and smad4 to critical TGF beta-inducible elements in the promoter of human plasminogen activator inhibitor-type 1 gene. *EMBO J.* 1998;17:3091–3100.
30. Zuk PA, Zhu M, Ashjian P, et al. Human adipose tissue is a source of multipotent stem cells. *Mol Biol Cell.* 2002;13:4279–4295.

31. Shayan R, Karnezis T, Tsantikos E, et al. A system for quantifying the patterning of the lymphatic vasculature. *Growth Factors.* 2007;25:417–425.
32. Livesey SA, Herndon DN, Hollyoak MA, et al. Transplanted acellular allograft dermal matrix. Potential as a template for the reconstruction of viable dermis. *Transplantation.* 1995;60:1–9.
33. Liao Y, Smyth GK, Shi W. The subread aligner: fast, accurate and scalable read mapping by seed-and-vote. *Nucleic Acids Res.* 2013;41:e108.
34. Robinson MD, McCarthy DJ, Smyth GK. Edger: a bioconductor package for differential expression analysis of digital gene expression data. *Bioinformatics.* 2010;26:139–140.
35. Smyth GK, Michaud J, Scott HS. Use of within-array replicate spots for assessing differential expression in microarray experiments. *Bioinformatics.* 2005;21:2067–2075.
36. Law CW, Chen Y, Shi W, et al. Voom: precision weights unlock linear model analysis tools for RNA-seq read counts. *Genome Biol.* 2014;15:R29.
37. Smyth GK. Linear models and empirical bayes methods for assessing differential expression in microarray experiments. *Stat Appl Genet Mol Biol.* 2004;3:Article3.
38. Benjamini Y, Hochberg Y. Controlling the false discovery rate: a practical and powerful approach to multiple testing. *Journal of the Royal Statistical Society Series B (Methodological).* 1995;57:289–300.
39. Luwor RB, Wang B, Nheu TV, et al. New reagents for improved *in vitro* and *in vivo* examination of TGF-β signalling. *Growth Factors.* 2011;29:211–218.
40. Larsson O, Diebold D, Fan D, et al. Fibrotic myofibroblasts manifest genome-wide derangements of translational control. *PLoS One.* 2008;3:e3220.
41. Warters RL, Packard AT, Kramer GF, et al. Differential gene expression in primary human skin keratinocytes and fibroblasts in response to ionizing radiation. *Radiat Res.* 2009;172:82–95.
42. Randall K, Coggle JE. Expression of transforming growth factor-beta 1 in mouse skin during the acute phase of radiation damage. *Int J Radiat Biol.* 1995;68:301–309.
43. Herskind C, Johansen J, Bentzen SM, et al. Fibroblast differentiation in subcutaneous fibrosis after postmastectomy radiotherapy. *Acta Oncol.* 2000;39:383–388.
44. Rodemann HP, Blaese MA. Responses of normal cells to ionizing radiation. *Semin Radiat Oncol.* 2007;17:81–88.
45. Rodier F, Campisi J. Four faces of cellular senescence. *J Cell Biol.* 2011;192:547–556.
46. Coppé JP, Kauser K, Campisi J, et al. Secretion of vascular endothelial growth factor by primary human fibroblasts at senescence. *J Biol Chem.* 2006;281:29568–29574.
47. Seluanov A, Gorbunova V, Falcovitz A, et al. Change of the death pathway in senescent human fibroblasts in response to DNA damage is caused by an inability to stabilize p53. *Mol Cell Biol.* 2001;21:1552–1564.
48. Walter MN, Wright KT, Fuller HR, et al. Mesenchymal stem cell-conditioned medium accelerates skin wound healing: an *in vitro* study of fibroblast and keratinocyte scratch assays. *Exp Cell Res.* 2010;316:1271–1281.
49. Hei TK, Zhou H, Ivanov VN, et al. Mechanism of radiation-induced bystander effects: a unifying model. *J Pharm Pharmacol.* 2008;60:943–950.
50. Raftopoulou M, Hall A. Cell migration: rho gtpases lead the way. *Dev Biol.* 2004;265:23–32.
51. Autio P, Saarto T, Tenhunen M, et al. Demonstration of increased collagen synthesis in irradiated human skin in vivo. *Br J Cancer.* 1998;77:2331.
52. Saad S, Stanners SR, Yong R, et al. Notch mediated epithelial to mesenchymal transformation is associated with increased expression of the snail transcription factor. *Int J Biochem Cell Biol.* 2010;42:1115–1122.
53. Cox TR, Erler JT. Remodeling and homeostasis of the extracellular matrix: implications for fibrotic diseases and cancer. *Dis Model Mech.* 2011;4:165–178.
54. el Nabout R, Martin M, Remy J, et al. Collagen synthesis and deposition in cultured fibroblasts from subcutaneous radiation-induced fibrosis. Modification as a function of cell aging. *Matrix.* 1989;9:411–420.
55. Abreu-Velez AM, Howard MS. Collagen IV in normal skin and in pathological processes. *N Am J Med Sci.* 2012;4:1–8.
56. Ricard-Blum S. The collagen family. *Cold Spring Harb Perspect Biol.* 2011;3:a004978.
57. Villone D, Fritsch A, Koch M, et al. Supramolecular interactions in the dermo-epidermal junction zone: anchoring fibril-collagen VII tightly binds to banded collagen fibrils. *J Biol Chem.* 2008;283:24506–24513.
58. Goessler UR, Bugert P, Kassner S, et al. *In vitro* analysis of radiation-induced dermal wounds. *Otolaryngol Head Neck Surg.* 2010;142:845–850.
59. Mueller H, Kassack MU, Wiese M. Comparison of the usefulness of the MTT, ATP, and calcein assays to predict the potency of cytotoxic agents in various human cancer cell lines. *J Biomol Screen.* 2004;9:506–515.
60. Yang YC, Piek E, Zavadil J, et al. Hierarchical model of gene regulation by transforming growth factor. *Proc Natl Acad Sci U S A.* 2011;100:10269–10274.
61. Roberts A, Tian F, Byfield S, et al. Smad3 is key to TGF-β-mediated epithelial-to-mesenchymal transition, fibrosis, tumor suppression and metastasis. *Cytokine Growth Factor Rev.* 2006;17:19–27.